

## Critical Point of the $^{152}\text{Sm}$ , $^{154}\text{Gd}$ , and $^{156}\text{Dy}$ Isotones

**Mushtaq Abed Al-Jubbori<sup>1)</sup>\*, **Huda H. Kassim<sup>2)</sup>**, **Fahmi Sh. Radhi<sup>3)</sup>**,  
**Amin Attarzadeh<sup>4)</sup>**, **I. Hossain<sup>5)</sup>**, **Imad M. Ahmed<sup>1)</sup>**, and **Fadhil I. Sharrad<sup>2),6)</sup>\*\*****

Received November 13, 2018; revised November 13, 2018; accepted January 11, 2019

**Abstract**—The even–even rare–earth nuclei in  $U(5)$ – $SU(3)$  region at neutron number ( $N$ ) = 90, have been systematically studied using the Bohr–Mottelson Model (BM), Interacting Vector Boson Model (IVBM), and Interacting Boson Model (IBM). The positive ground-state band (GSB) of  $^{152}\text{Sm}$ ,  $^{154}\text{Gd}$ , and  $^{156}\text{Dy}$  nuclei has been calculated by using BM, IVBM, and IBM, while the negative-parity band (NPB) of those nuclei are calculated by BM and IVBM only. To determine the intermediate structure, the ratio  $(r(I+2)/I)$  and  $E$ -GOS curve ( $E$ -Gamma Over Spin) as a function of the spin ( $I$ ) have been drawn. In the IBM, the calculated reduced  $B(E2)$  transition probabilities of the GSB in the  $^{152}\text{Sm}$ ,  $^{154}\text{Gd}$ , and  $^{156}\text{Dy}$  nuclei are analyzed and compared to the prediction of vibrational  $U(5)$  and rotational  $SU(3)$  limits. In the Sm–Dy nuclei with  $N = 90$ , the  $U(5)$ – $SU(3)$  IBM potential energy surfaces (PES's) are analyzed and evolve from spherical to deformed shapes with increasing the boson number. The critical phase transition points are identified in the space of model parameters and  $^{152}\text{Sm}$ ,  $^{154}\text{Gd}$ , and  $^{156}\text{Dy}$  nuclei have been found to be close to critical points.

**DOI:** 10.1134/S1063778819030049

### 1. INTRODUCTION

In recent years, the phase transition between spherical and axially deformed quadrupole shapes of nuclei has been the object of several theoretical and experimental works and there have been many attempts to explore the factors responsible for the onset of large deformation in nuclei of the mass region  $A \geq 150$ . The even–even Sm–Dy nuclei span an interesting section of the nuclear chart close to the well-known transitional region from spherical to axially deformed shapes of the rare–earth nuclei. In the case of Sm–Dy,  $N = 90$ , there are fewer neutrons outside the major closed shell ( $N = 82$ ) and the study of these nuclei provides us with an insight into the effect that this might have on the transition from  $U(5)$  to  $SU(3)$  symmetry. Many models have been developed to describe collective properties of nuclei.

For an example, the geometric model of Bohr and Mottelson (BM) which found an interpretation of the vibrations in many nuclei that are associated with (mainly quadrupole) oscillations of the nuclear surface and they introduced a relation of the rotational energy  $E$  of an axially symmetric nucleus as a function of  $I(I+1)$  [1]. With the advent of the Interacting Boson Model (IBM-1) [2], the IBM reveals rich features of their shape phase transitions [3–6] and three dynamical symmetries in the IBM were shown to correspond to three typical shape phase of nuclei, known  $U(5)$ ,  $SU(3)$ , and  $O(6)$  [7, 8], corresponding to the three limiting symmetries of the collective model, viz. spherical vibrator, axially symmetric deformed rotor, and  $\gamma$ -unstable, respectively. It became easier to study the nuclear structure of medium and heavy mass nuclei. Phase transitions between these shapes which are known as phase transition from a vibrator to axial rotor and to a  $\gamma$ -unstable rotor, are called  $X(5)$  and  $E(5)$ , respectively. It was first introduced by Iachello [9, 10]. The Interacting Vector Boson Model (IVBM) introduced in the beginning of the 1980s was based on two kinds of vector bosons, the proton  $p$  and neutron  $n$  bosons that constitute the collective excitations in the nucleus. The IVBM has been developed by Ganev et al. [11, 12] to describe the ground and octupole bands of the nucleus. In even nuclei exhibiting octupole deformation the ground-state band, which contains energy levels with  $I^\pi = 0^+, 2^+, 4^+, \dots$  is accompanied by a negative parity

<sup>1)</sup>Department of Physics, College of Education for Pure Science, University of Mosul, Iraq.

<sup>2)</sup>Department of Physics, College of Science, University of Kerbala, Iraq.

<sup>3)</sup>Department of Physics, College of Education for Pure Science, University of Basrah, Iraq.

<sup>4)</sup>Institute for Higher Education ACECR, Khuzestan, Iran.

<sup>5)</sup>Department of Physics, Rabigh College of Science and Arts, King Abdulaziz University, Saudi Arabia.

<sup>6)</sup>College of Health and Medical Technology, Al-Ayen University, Al Nasiriya, Thi Qar, Iraq.

\*E-mail: mushtaq\_phy8@yahoo.com

\*\*E-mail: fadhil.altai@gmail.com

band containing energy levels with  $I^\pi = 1^-, 3^-, 5^-, \dots$ . After the first few values of angular momentum  $I$  the two bands become interwoven, forming a single octupole band with levels characterized by  $I^\pi = 0^+, 1^-, 2^+, 3^-, 4^+, \dots$  [1, 13–17], while a negative parity band lying systematically higher than the ground state band is a footprint of octupole vibrations.

Many experimental and theoretical studies on the structure of energy level and electromagnetic transition properties of the even–even rare-earth nuclei have been investigated [18–26]. Recently, in the same region of  $U(5)$ – $SU(3)$ , some nuclei have been studied like Ba–Dy nuclei at  $N = 92$  [27], even–even  $^{154-164}\text{Gd}$  isotopes [28] and Er–Os nuclei for  $N = 100$  [29].

In the present work, by application of BM, IVBM, and IBM-1 to predict the low positive excitation states of  $^{152}\text{Sm}$ ,  $^{154}\text{Gd}$ , and  $^{156}\text{Dy}$  nuclei and the calculations of negative-parity state energies of these nuclei have been studied using BM and IVBM. By using IBM-1, the reduced transition probabilities  $B(E2)$  of these nuclei are calculated and compared with their experimental counterparts. The potential surface energy is plotted for these nuclei.

## 2. METHOD OF CALCULATIONS

In the Bohr–Mottelson nuclear model, the energy expansion (GSB and the NPB levels) for deformed nuclei in the powers  $I(I+1)$  are given by [1, 30, 31]:

$$E(I) = AI(I+1) - BI^2(I+1)^2 + CI^3(I+1)^3, \quad (1)$$

$$E(I) = E_0 + A'I(I+1) - B'I^2(I+1)^2 + C'I^3(I+1)^3, \quad (2)$$

where  $E_0$  is the band head energy of the NPB and the coefficients  $A > A'$ ,  $B > B'$ , and  $C > C'$  can be determined from a fit to the available energy levels of this band.

The eigenvalues for the GSB and NPB states in IVBM model are given by [11, 32]

$$E(I) = \beta I(I+1) + \gamma I, \quad (3)$$

$$E(I) = \beta I(I+1) + (\gamma + \eta)I + \zeta. \quad (4)$$

The values of  $\beta$  and  $\gamma$  can be determined from a fit to the positive GSB, while  $\eta$  and  $\zeta$  are estimated from the negative ones.

No distinction is made between proton and neutron degrees of freedom in the original formulation of the interacting boson model. In even–even nuclei, the low-lying collective states are described in terms of a system of  $N_b$  interacting bosons with angular

momentum and parity  $L = 0^+$  (monopole) and  $L = 2^+$  (quadrupole).

The IBM-1 Hamiltonian can be expressed as [2, 7, 33]:

$$\begin{aligned} H = & \varepsilon_s(s^\dagger \tilde{s}) + \varepsilon_d(d^\dagger \tilde{d}) \\ & + \sum_{L=0,2,4} \frac{1}{2} (2L+1)^{\frac{1}{2}} C_L \\ & \times \left[ [d^\dagger \times d^\dagger]^{(L)} \times [\tilde{d} \times \tilde{d}]^{(L)} \right]^{(0)} \\ & + \frac{1}{\sqrt{2}} v_2 \left[ [d^\dagger \times d^\dagger]^{(2)} \times [\tilde{d} \times \tilde{s}]^{(2)} \right. \\ & \left. + [d^\dagger \times s^\dagger]^{(2)} \times [\tilde{d} \times \tilde{d}]^{(2)} \right]^{(0)} \\ & + \frac{1}{2} v_0 \left[ [d^\dagger \times d^\dagger]^{(0)} \times [\tilde{s} \times \tilde{s}]^{(0)} \right. \\ & \left. + [s^\dagger \times s^\dagger]^{(0)} \times [\tilde{d} \times \tilde{d}]^{(0)} \right]^{(0)} \\ & + \frac{1}{2} u_0 \left[ [s^\dagger \times s^\dagger]^{(0)} \times [\tilde{s} \times \tilde{s}]^{(0)} \right]^{(0)} \\ & + u_2 \left[ [d^\dagger \times s^\dagger]^{(2)} \times [\tilde{d} \times \tilde{s}]^{(2)} \right]^{(0)}. \end{aligned} \quad (5)$$

The full Hamiltonian  $H$  contains six adjustable parameters, and can be written as [33, 34]:

$$\hat{H} = \varepsilon \hat{n}_d + a_0 \hat{p} \hat{p} + a_1 \hat{L} \hat{L} + a_2 \hat{Q} \hat{Q} + a_3 \hat{T}_3 \hat{T}_3 + a_4 \hat{T}_4 \hat{T}_4, \quad (6)$$

where  $\varepsilon$  is the boson energy, and the operators are:

$$\left. \begin{aligned} \hat{n}_d &= (d^\dagger \tilde{d}), \\ \hat{p} &= 1/2[(\tilde{d} \tilde{d}) - (\tilde{s} \tilde{s})], \\ \hat{L} &= \sqrt{10}[d^\dagger \times \tilde{d}]^1, \\ \hat{Q} &= [d^\dagger \times \tilde{s} + s^\dagger \times \tilde{d}]^{(2)} + \chi [d^\dagger \times \tilde{d}]^{(2)}, \\ \hat{T}_r &= [d^\dagger \times \tilde{d}]^{(r)}. \end{aligned} \right\} \quad (7)$$

Here,  $\hat{n}_d$  is the total number of  $d_{\text{boson}}$  operators,  $\hat{p}$  is the pairing operator,  $\hat{L}$  is the angular momentum operator and  $\hat{T}_r$  is the octupole ( $r = 3$ ) and hexadecapole ( $r = 4$ ), while the operator  $\hat{Q}$  is the quadrupole operator ( $\chi$  is the quadrupole structure parameter and takes the values 0 and  $\pm \frac{\sqrt{7}}{2}$  [35–37]). However, the total number of boson  $N_b$  (pairs) is conserved,  $N_b = n_s + n_d$  [33] and  $a_0$ ,  $a_1$ ,  $a_2$ ,  $a_3$ , and  $a_4$  are the strengths of pairing, angular momentum, quadrupole,

octupole and hexadecupole interactions of each term in the Eq (6).

For some nuclei, the positive parity yrast levels are connected by a sequence of stretched  $E2$  transitions with energies from a state with  $I$  to a state with  $I-2$  except around the back-bends while a dramatic change in the moment of inertia  $\vartheta$  may occur by increasing the angular momentum  $I$ . This behavior causes back (or up)-bending in the value of the energy  $\hbar\omega$  which is given by [31, 38–40]:

$$\hbar\omega = \frac{E_\gamma}{\sqrt{I(I+1)} - \sqrt{(I-2)(I-1)}}. \quad (8)$$

The relation between the moment of inertia ( $\vartheta$ ) and gamma energy  $E_\gamma$  is given by [41]:

$$2\vartheta/\hbar^2 = \frac{4I-2}{E(I)-E(I-2)} = \frac{4I-2}{E_\gamma}. \quad (9)$$

For each spin  $I$  in a given band, the following ratios were constructed to define the symmetry for the excited band of even–even nuclei using Eq. (10) [42–45]:

$$r\left(\frac{I+2}{I}\right) = \left[ R\left(\frac{I+2}{I}\right)_{\text{exp}} - \frac{(I+2)}{I} \right] \frac{I(I+1)}{2(I+2)}, \quad (10)$$

where  $R\left(\frac{I+2}{I}\right)_{\text{exp}}$  is the ratio of the experimental energy values between  $I+2$  and  $I$  states. In Eq. (10), the values of ( $r$ ) are ranging from 0.1 to 1.0 for yrast bands of even–even nuclei. The ratio of ( $r$ ) for the vibrational nucleus should be close to zero, close to one for rotational nucleus while in  $\gamma$ -unstable nuclei, it should have intermediate values and be given by [43, 46]:  $0.1 \leq r \leq 0.35$  for vibrational nuclei,  $0.4 \leq r \leq 0.6$  for transitional nuclei and  $0.6 \leq r \leq 1.0$  for rotational nuclei.

The characteristics of the nucleus along its excited states identity, are discussed and changes are discerned by plotting the ratio of  $E(I)$  as a function of spin ( $E$ -GOS) [47–49]. The relations between ( $R = E_\gamma/I$ ) and the angular momentum  $I$  for the three limits are given by [50, 51]:

$$U(5): \quad R = \frac{\hbar\omega}{I} \rightarrow 0 \quad \text{when} \quad I \rightarrow \infty, \quad (11)$$

$$O(6): \quad R = \frac{E2_1^+}{4} \left(1 + \frac{2}{I}\right) \rightarrow \frac{E2_1^+}{4} \quad (12)$$

when  $I \rightarrow \infty$ ,

$$SU(3): \quad R = \frac{\hbar^2}{2\vartheta} \left(4 - \frac{2}{I}\right) \rightarrow \frac{4\hbar^2}{2\vartheta} \quad (13)$$

when  $I \rightarrow \infty$ .

Through using the expression  $\Delta E_{1,\gamma}(I)$  ( $\Delta I = 1$  staggering) in Eq. (14) (see below), odd–even staggering patterns in octupole bands have been investigated [16, 52, 53] and take alternatively positive and negative values of equal absolute value as  $I$  increases and are given as:

$$\Delta E_{1,\gamma}(I) = 1/16[6E_{1,\gamma}(I) - 4E_{1,\gamma}(I-1) - 4E_{1,\gamma}(I+1) + E_{1,\gamma}(I-2) + E_{1,\gamma}(I+2)], \quad (14)$$

where

$$E_{1,\gamma}(I) = E_{1,\gamma}(I+1) - E(I). \quad (15)$$

In the evolution of nuclear structure, phase transitional behavior from spherical to deformed shapes within the framework of the Interacting Boson Model can be studied through the coherent state formalism ( $|N_b, \beta, \gamma\rangle$ ) and this technique described by Dieperink et al. [54]. By using the intrinsic coherent state formalism, the potential energy surfaces to the IBM Hamiltonian [2] have been obtained which yields a function of shape variables  $\beta$  and  $\gamma$  which is given as [2, 33, 55, 56]:

$$E(N_b, \beta, \gamma) = \frac{\langle N, \beta, \gamma | H | N, \beta, \gamma \rangle}{\langle N, \beta, \gamma | N, \beta, \gamma \rangle}. \quad (16)$$

Simpler expressions, which display the essential dependence on  $\beta$  and  $\gamma$ , have been given by [33, 35]:

$$E(N_b, \beta, \gamma) = \varepsilon N_b [\beta^2 / (1 + \beta^2)] \dots U(5), \quad (17)$$

$$E(N_b, \beta, \gamma) = a_2 N_b (N_b - 1) [(1 + 3/4\beta^4 - \sqrt{2}\beta^3 \cos 3\gamma) / (1 + \beta^2)^2] \dots SU(3), \quad (18)$$

$$E(N_b, \beta, \gamma) = a_0 N_b (N_b - 1) [(1 - \beta^2) / (1 + \beta^2)]^2 \dots O(6). \quad (19)$$

Here  $\beta \geq 0$  and  $0 \leq \gamma \leq \pi/3$  are intrinsic shape parameters which determine the geometrical shape of the nucleus and the expression give (for large  $N_b$ )  $\beta_{\text{min}} = 0, \sqrt{2}$ , and 1 for  $U(5)$ ,  $SU(3)$ , and  $O(6)$ , respectively [33, 57, 58].

### 3. RESULTS AND DISCUSSION

The first-order phase transition between spherical  $U(5)$  and axially deformed  $SU(3)$  shapes [9] has received widespread attention in the past decade. In this paper, the even–even rare-earth nuclei ( $N = 90$ )  $^{62}\text{Sm}$ ,  $^{64}\text{Gd}$ , and  $^{66}\text{Dy}$  have been studied, through displaying first-order phase transition from spherically to axial symmetric deformed  $U(5)$ – $SU(3)$ .  $^{152}\text{Sm}$ ,  $^{154}\text{Gd}$ , and  $^{156}\text{Dy}$  nuclei have neutron number  $N = 90$  and have an even atomic number  $Z = 62$  to 66 ( $Z$  and  $N$  values near mid shell and  $N$  value

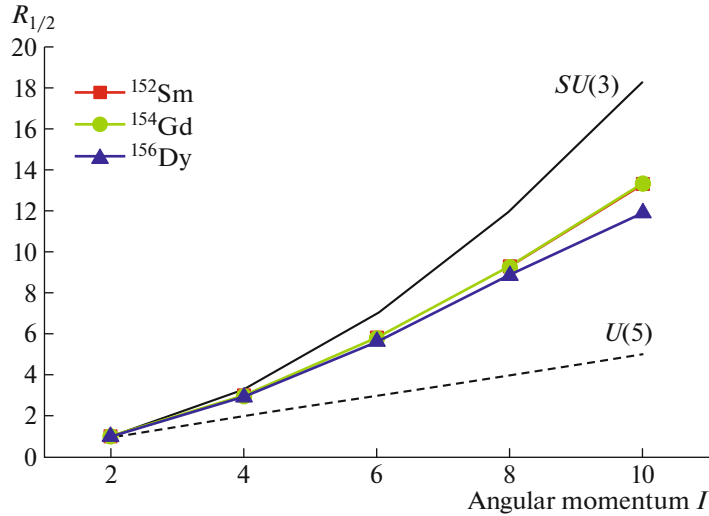


Fig. 1. The energy ratio  $R_{I/2}$  in  $^{152}\text{Sm}$ ,  $^{154}\text{Gd}$ , and  $^{156}\text{Dy}$  nuclei [64–67] versus spin  $I$ .

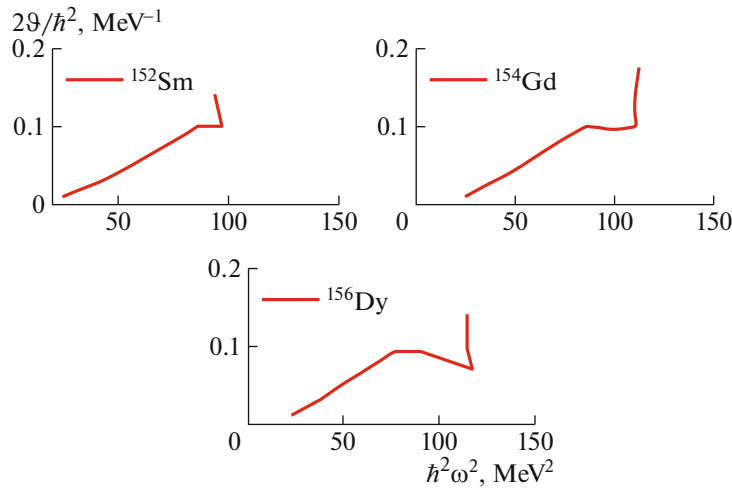


Fig. 2. Back (or up)-bending of the ground state band for  $^{152}\text{Sm}$ ,  $^{154}\text{Gd}$ , and  $^{156}\text{Dy}$  nuclei [64–67].

near closed shell would suggest the  $U(5)$ – $SU(3)$  transition structure). Phase transitions in nuclei can be tested by calculating the energy ratios [59, 60]:

$$R_{I/2} = E_{I_1^+}/E_{2_1^+}. \quad (20)$$

For  $I = 4$ , the ratio  $R_{4/2} = E_{4_1^+}/E_{2_1^+}$  varied from the values which correspond to vibrations around a spherical shape  $R_{4/2} = 2, 2.5$  for  $\gamma$ -unstable nuclei,  $\sim 2.2$  for the analytically solvable symmetry  $E(5)$  on the  $U(5)$ – $O(6)$  path,  $\sim 2.9$  for the approximate  $X(5)$  symmetry on the  $U(5)$ – $SU(3)$  path and to the characteristic value for excitations of a well-deformed rotor  $R_{4/2} = 10/3$  [9, 10, 61–63]. Figure 1 shows the  $R_{I/2}$  for  $^{152}\text{Sm}$ ,  $^{154}\text{Gd}$ , and  $^{156}\text{Dy}$  nuclei compared to  $U(5)$  and  $SU(3)$  prediction and show the slope  $R_{I/2}$  is stable with increasing  $Z$ , indicating the property

between vibrational and quadrupole deformation, i.e. the  $X(5)$  property for  $^{152}\text{Sm}$ ,  $^{154}\text{Gd}$ , and  $^{156}\text{Dy}$  nuclei.

The back (or up)-bending curves,  $r\left(\frac{I+2}{I}\right)$ , the  $E$ -GOS curves and the staggering phenomena are used to ensure the properties of these nuclei along their ground state band. The rotational frequency  $\hbar\omega$  and moment of inertia  $2\vartheta/\hbar^2$  have been calculated from (8) and (9), respectively.

In Fig. 2, the moments of inertia  $2\vartheta/\hbar^2$  are plotted versus the square of rotational energy  $\hbar\omega$  of the photons emitted during the transition between the different states. There is a back-bending curvature that occurred in the  $\hbar\omega$  value of the Sm–Dy nuclei for  $N = 90$ . The ratio  $r((I+2)/I)$  as a function of  $I$  for the ground state bands of these nuclei are drawn.

**Table 1.** The BM, IVBM and IBM-1 parameters of GSB in MeV except  $N_b$  and CHQ for  $^{152}\text{Sm}$ ,  $^{154}\text{Gd}$ , and  $^{156}\text{Dy}$  nuclei

Nucleus	$N_b$	BM			IVBM		IBM-1			
		$A \times 10^{-2}$	$B \times 10^{-5}$	$C \times 10^{-8}$	$\beta \times 10^{-3}$	$\gamma \times 10^{-2}$	EPS	ELL	QQ	CHQ
$^{152}\text{Sm}$	10	1.8484	4.4041	8.6305	9.8290	4.9978	0.033	0.0313	-0.024	-2.958
$^{154}\text{Gd}$	11	1.8735	4.3748	8.3648	9.9705	5.0968	0.100	0.0327	-0.0218	-2.958
$^{156}\text{Dy}$	12	2.0356	5.3436	10.506	9.8724	6.0537	0.065	0.0381	-0.0201	-2.958

ELL =  $2a_1$  and QQ =  $2a_2$ , CHQ =  $\sqrt{5}\chi$  [33].

**Table 2.** The BM and IVBM parameters of NPB in MeV  $^{152}\text{Sm}$ ,  $^{154}\text{Gd}$ , and  $^{156}\text{Dy}$  nuclei

Nucleus	BM				IVBM	
	$A' \times 10^{-3}$	$B' \times 10^{-6}$	$C' \times 10^{-9}$	$E_0$	$\zeta$	$\eta$
$^{152}\text{Sm}$	12.959	18.726	27.678	0.96336	1.2413	-0.0413
$^{154}\text{Gd}$	9.9494	1.6741	-0.47149	1.2413	1.2425	-0.0473
$^{156}\text{Dy}$	10.405	3.9117	1.7211	1.2932	0.9771	-0.0424

Figure 3 shows the relationship between the ratio  $r$  and the spin  $I$  and gives numerical values which insure the properties of each nucleus. According to Fig. 3, this study supports the interpretation of the critical point of  $^{152}\text{Sm}$ ,  $^{154}\text{Gd}$ , and  $^{156}\text{Dy}$  nuclei. Hence, the  $^{152}\text{Sm}$ ,  $^{154}\text{Gd}$ , and  $^{156}\text{Dy}$  nuclei are associated to  $X(5)$  symmetry when the ratio  $r((I + 2)/I)$  started with high value  $\geq 0.755$  and then decreases with  $I$  to  $>0.5$ .

In Fig. 4a, the  $E$ -GOS curve presents the theoretical limits for three schematic nuclei plotted and shown: (i) a vibrator, which the sharp hyperbolic decrease in  $R$  with spin  $I$ , (ii)  $R$  decreases with  $I$  in  $\gamma$ -soft nucleus but at a slower rate than for a vibrator; and by contrast (iii) a rotor,  $R$  actually increases at low spins.

Figure 4b shows the  $E$ -GOS curves of the positive parity yrast band of even-even Sm-Dy nuclei with  $N = 90$  compared with the ideal limits of vibrational, rotational, and  $\gamma$ -soft shown in Fig. 4a. Normally, the Sm-Dy nuclei in Fig. 4b show the sharp drop of the  $E$ -GOS curve and these positive parity yrast bands have good rotational characteristic in the spin region ( $I = 4$  to 8), while it has good vibrational characteristic in the higher-spin region above  $I \geq 10$ . So, it is interesting to see that the  $E$ -GOS curve occurrence between the two standard curves of  $U(5)$  and  $SU(3)$  giving these nuclei the  $X(5)$  properties.

The apparent staggering in the differences between the energies of GSB and NPB is shown in

Fig. 5 for  $^{152}\text{Sm}$ ,  $^{154}\text{Gd}$ , and  $^{156}\text{Dy}$  nuclei. In this figure, the decrease of the staggering with increasing  $I$ , approach to zero at spin above 10 and then the increase of the staggering with increasing  $I$  which confirms the phase change of this nuclei. Taking the above studies all together gives the  $U(5)$ - $SU(3)$  properties.

In Sm-Dy nuclei with  $N = 90$ , the BM, IVBM were used to calculate the energy states in GSB and NPB with MATLAB 7.0 software and IBM-1 was used to calculate the energy states in GSB only with PHINT code [68]. The BM, IBM-1, and IVBM parameters of GSB for these nuclei, the number of bosons  $N_b$  (calculated from the sum of the proton bosons of the close shells (50 and 82) and the neutron bosons of the close shells (82 and 126)) and the best values of the parameters which give the best fitting between theoretical and the experimental energy levels (GSB) of the above nuclei are presented in Table 1. Table 2 shows the BM and IVBM parameters of NPB which give the best fitting to the experimental excited states. The octupole bands within the IBM realm can be described in the framework of the spdf-IBM, introduced by Engel and Iachello [48, 49] and further are developed by Kusnezov and Zamfir [30, 69-71]. The explicit expression of Hamiltonian [2, 33, 72] is adopted in the calculations using the following equation:

$$\hat{H} = \varepsilon \hat{n}_d + a_1 \hat{L}\hat{L} + a_2 \hat{Q}\hat{Q} \quad (21)$$

for  $U(5) - SU(3)$ .

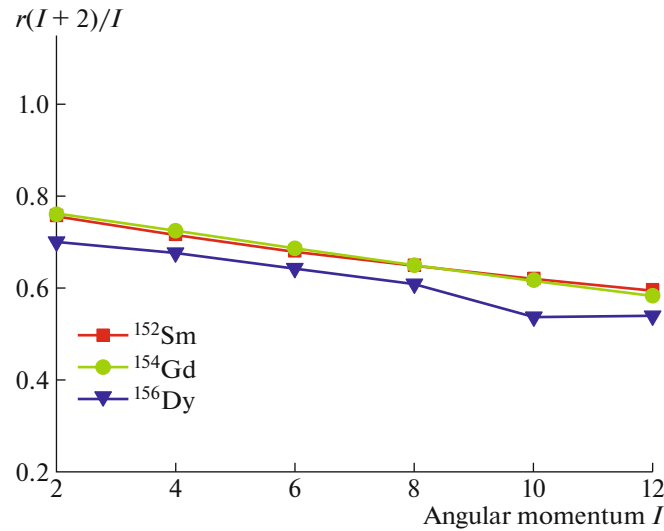


Fig. 3. The ratio  $r\left(\frac{I+2}{I}\right)$  as a function of  $I$  for  $^{152}\text{Sm}$ ,  $^{154}\text{Gd}$ , and  $^{156}\text{Dy}$  nuclei [64–67].

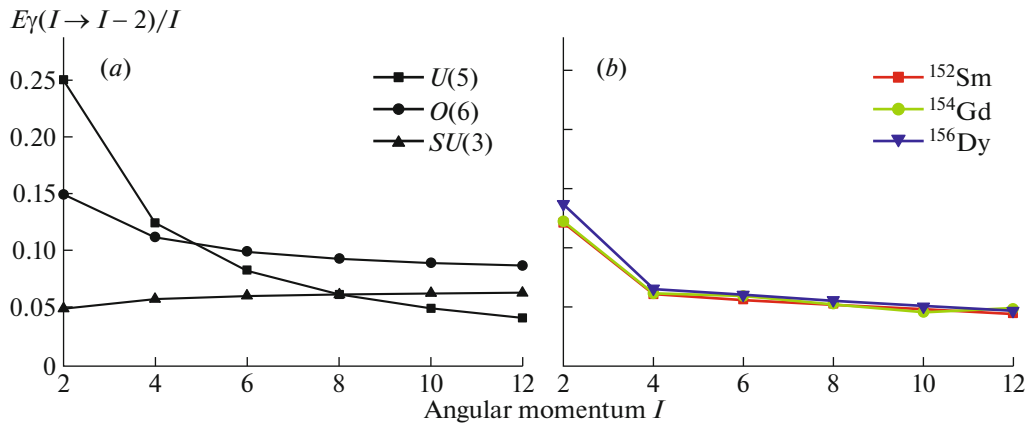


Fig. 4. (a)  $E$ -GOS curves for a perfect harmonic vibrator,  $\gamma$ -soft and axially-symmetric rotor, (b)  $E$ -GOS curves of the GSB for  $^{152}\text{Sm}$ ,  $^{154}\text{Gd}$ , and  $^{156}\text{Dy}$  nuclei [64–67].

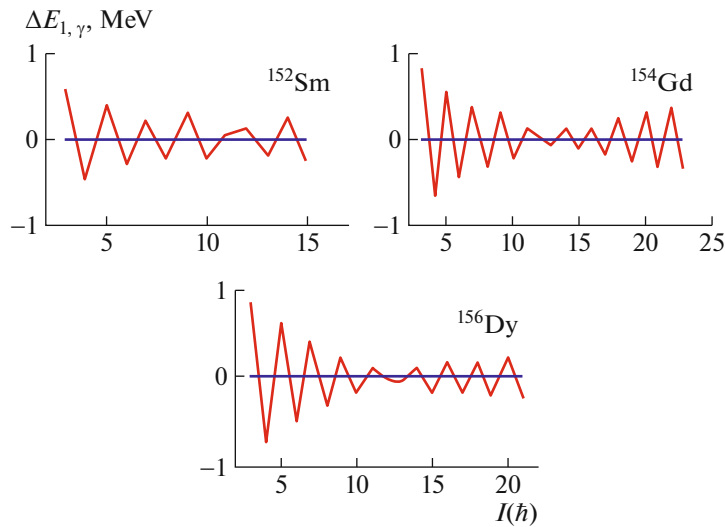
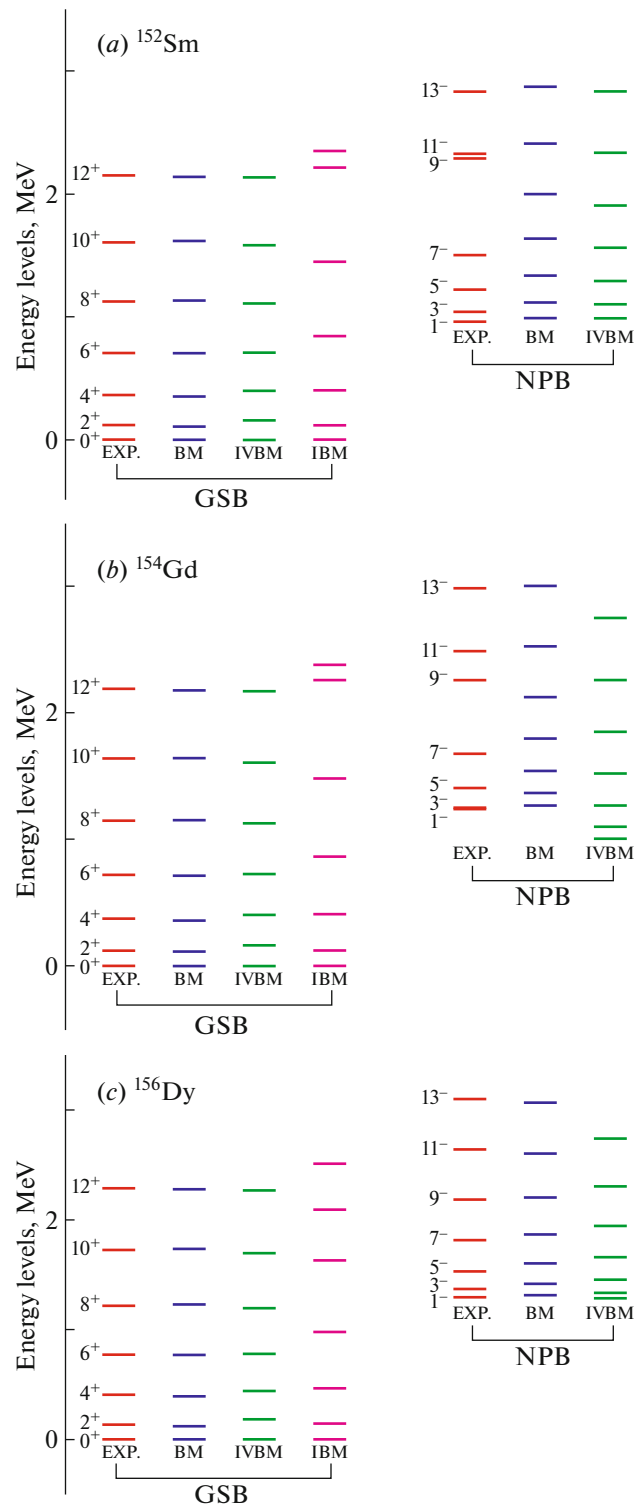


Fig. 5. Staggering for  $^{152}\text{Sm}$ ,  $^{154}\text{Gd}$ , and  $^{156}\text{Dy}$  nuclei [64–67].

The calculated and experimental energies [64–67] of GSB and NPB of Sm–Dy are plotted in Fig. 6a, 6b, and 6c and it is shown that the energy levels (GSB

and NPB) rise continuously with increasing  $I$  while  $N$  is constant ( $N = 90$ ) for all the selected rare-earth nuclei.



**Fig. 6.** Comparison of the BM, IVBM, and IBM-1 energy level calculations with the available experimental data [64–67] in GSB and NPB for  $^{152}\text{Sm}$  (a),  $^{154}\text{Gd}$  (b), and  $^{156}\text{Dy}$  nuclei (c).

In Fig. 6a, 6b, and 6c, the calculated energy levels are in good agreement with experimental ones for all these nuclei and for all states with some deviation for

NPB states in  $^{152}\text{Sm}$  and  $^{154}\text{Gd}$  due to the big gap between 7 state and 9 state for these nuclei, which are different from  $^{156}\text{Dy}$  nuclei. In general, the calcu-

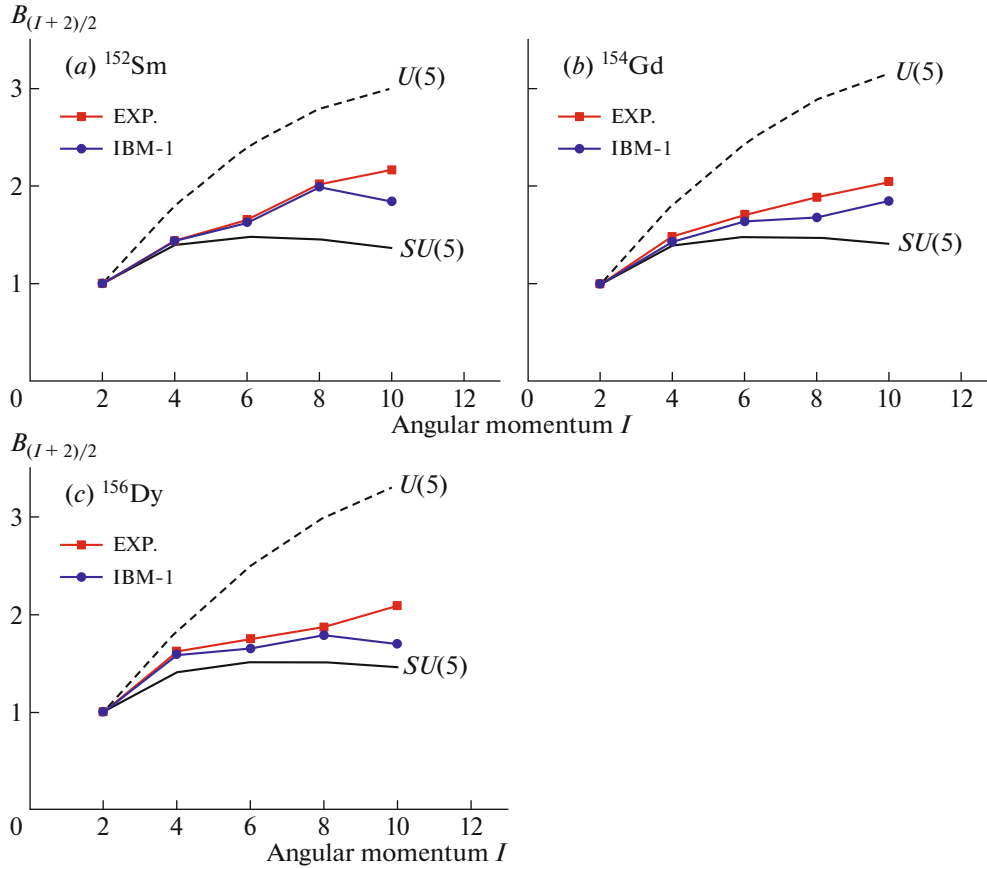


**Fig. 7.** Comparison of the  $B_{(I+2)/2}$  calculations with the experimental ratio of GSB for  $^{152}\text{Sm}$  (a),  $^{154}\text{Gd}$  (b), and  $^{156}\text{Dy}$  (c) nuclei.

lations of BM, IVBM predictions are in good agreement with the experimental values, while in IBM, the GSB deviated in the high angular momentum  $I$  from the experimental data (above  $I = 6$ ) for all rare-earth nuclei under this study.

The electric quadruple transition probabilities are the other key for studying and discussion of the other information on the structure of nuclei which can be expressed in terms of the reduced  $E2$  matrix element which must be a Hermiston tensor of rank two when  $N_b$  must be conserved. The electrical transition can be analyzed in the framework of the IBM, and the most general  $E2$  transition operator can be written as

**Table 3.** Parameters (in eb) used to reproduce  $B(E2)$  values for  $^{152}\text{Sm}$ ,  $^{154}\text{Gd}$ , and  $^{156}\text{Dy}$  nuclei

Nucleus	$N_b$	$e_B$
$^{152}\text{Sm}$	10	0.1230
$^{154}\text{Gd}$	11	0.1183
$^{156}\text{Dy}$	12	0.1074

[2, 33, 73, 74]:

$$T^{E2} = \alpha_2[d^\dagger s + s^\dagger d]^{(2)} + \beta_2[d^\dagger d]^{(2)} = e_B \hat{Q}, \quad (22)$$

where  $(s^\dagger, d^\dagger)$  and  $(s, d)$  are creation and annihilation operators for  $s$  and  $d$  bosons, respectively, while  $\alpha_2$  and  $\beta_2$  are two parameters, as  $(\beta_2 = \chi\alpha_2, \alpha_2 = e_B$  (effective charge of boson)) [33, 75, 76].

The reduced transition probability for the  $U(5)$  and  $O(6)$  limits are given by [33]:

$$U(5) \quad B(E2; L \rightarrow L-2) \quad (23) \\ = e_B^2 (n_d + 1) (N - n_d),$$

$$SU(3) \quad B(E2; L \rightarrow L-2) \quad (24) \\ = e_B^2 \frac{3(L+2)(L+1)}{4(2L+3)(2L+5)} (2N-L)(2N+L+3),$$

where  $L$  is the angular momentum. From the given and normalized predictions to the experimental value [64–67] of  $B(E2; 2_1^+ \rightarrow 0_1^+)$  transition, one can calculate the value of the effective charge  $e_B$  directly from using the above two equations for each isotope under this study and shown in Table 3. This value is

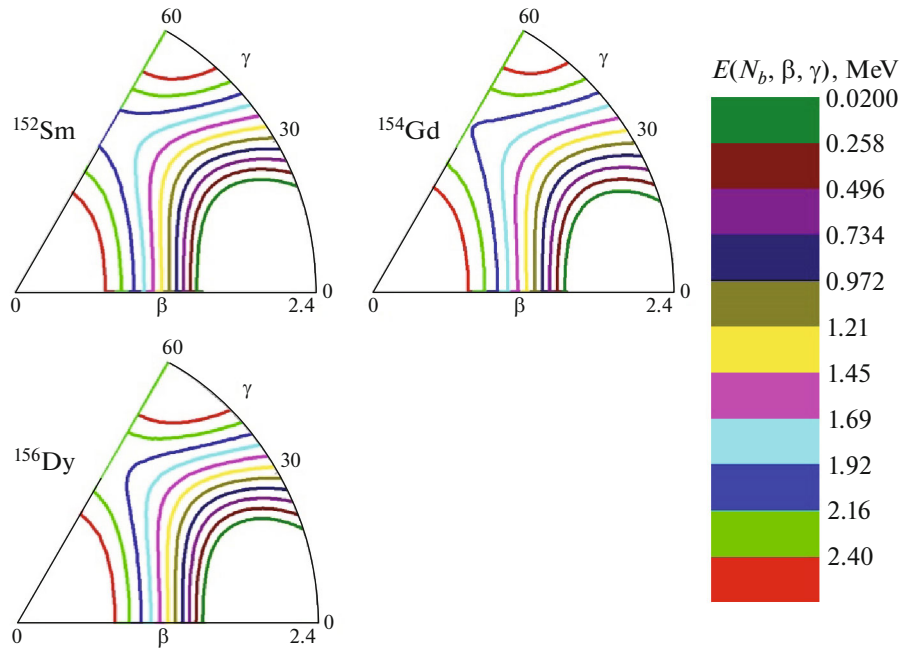


Fig. 8. The potential energy surfaces for  $^{152}\text{Sm}$ ,  $^{154}\text{Gd}$ , and  $^{156}\text{Dy}$  nuclei.

used to calculate the reduced transition probabilities  $B(E2; L \rightarrow L - 2)$  presented in Table 4.

Table 4 shows the  $B(E2)$  calculated values for the GSB with neutron number  $N = 90$  and compared with the experimental data [64–67] in Sm–Dy nuclei. It is shown that there is good agreement and strong consistency between the  $B(E2)$  calculated with experimental reports, except for few cases that deviate from the experimental data [64–67] in  $^{152}\text{Sm}$ ,  $^{154}\text{Gd}$ , and  $^{156}\text{Dy}$  nuclei.

The ratios  $B_{(I+2)/2} = (E2; I + 2 \rightarrow I) / (E2; 2_1^+ \rightarrow 0_1^+)$  of the  $E2$  transition rates for the  $U(5)$  and  $SU(3)$

are given by [2, 59]:

$$\left. \begin{aligned}
 B_{(I+2)/2} &= \frac{1}{2} (I + 2) \left( 1 - \frac{I}{2N} \right) \\
 \text{for } U(5), \\
 B_{(I+2)/2} &= \frac{15}{2} \frac{(I + 2)(I + 1)}{(2I + 3)(2I + 5)} \left( 1 - \frac{I}{2N} \right) \\
 &\times \left( 1 + \frac{I}{2N + 3} \right) \text{ for } SU(3).
 \end{aligned} \right\}$$

Table 4. The IBM-1 and Experimental [64–67] values of  $B(E2)$  (in  $e^2b^2$ ) of some states in the GSB for  $^{152}\text{Sm}$ ,  $^{154}\text{Gd}$ , and  $^{156}\text{Dy}$

Nucleus		$2_1^+ \rightarrow 0_1^+$	$4_1^+ \rightarrow 2_1^+$	$6_1^+ \rightarrow 4_1^+$	$8_1^+ \rightarrow 6_1^+$	$10_1^+ \rightarrow 8_1^+$
$^{152}\text{Sm}$	Exp.	0.699	1.001	1.157	1.412	1.513
	Cal.	0.694	1.000	1.127	1.234	1.180
$^{154}\text{Gd}$	Exp.	0.770	1.156	1.323	1.445	1.568
	Cal.	0.761	1.069	1.139	1.134	1.086
$^{156}\text{Dy}$	Exp.	0.748	1.211	1.311	1.402	1.546
	Cal.	0.743	1.146	1.221	1.323	1.281

The  $B_{(I+2)/2}$  ratios for the best candidate  $^{152}\text{Sm}$ ,  $^{154}\text{Gd}$ , and  $^{156}\text{Dy}$  compared to the  $U(5)$  and  $SU(3)$  predictions and the experimental data are shown in Fig. 7a, 7b, and 7c. Figures 7a, 7b, and 7c gives a good agreement between the IBM-1 and the experimental data [64–67], i.e. these nuclei have been found to be close to critical points.

In Fig. 8, the contour plots of the potential energy surfaces are presented and it is shown that Sm, Gd, and Dy nuclei under study have the shape phase transition from vibrational  $U(5)$  to rotational symmetry  $SU(3)$ .

#### 4. CONCLUSIONS

In the framework of BM, IVBM, and IBM, the positive ground-state band for the selected rare-earth nuclei in  $U(5)$ – $SU(3)$  region at the neutron number  $N = 90$  and the results are in good agreement with published experimental data. The back (or up)-bending curves, the ratio ( $r$ ), the  $E$ -GOS curves, and the staggering phenomena between GSB and NPB states are calculated to ensure the properties of these nuclei along their many excited states. The ratio  $(r(I+2)/I)$  and  $E$ -GOS curve ( $E_\gamma/I$ ) as a function of the spin ( $I$ ) are plotted and compared with the ideal limits of vibrational, rotational, and  $\gamma$ -soft and confirmed the  $X(5)$  property for  $^{152}\text{Sm}$ ,  $^{154}\text{Gd}$ , and  $^{156}\text{Dy}$  nuclei. Using Interacting Boson Model, the reduced transition probabilities  $B(E2)$  of these nuclei have been calculated and a good agreement was obtained with the published experimental data, except for few cases that deviate from the experimental data. The ratios  $B_{(I+2)/2} = (E2; I+2 \rightarrow I) / (E2; 2_1^+ \rightarrow 0_1^+)$  of the  $E2$  transition are plotted for  $^{152}\text{Sm}$ ,  $^{154}\text{Gd}$ , and  $^{156}\text{Dy}$  and show these nuclei have been found to be close to critical points. The contour plots of PES show that the shape phase transitions from  $U(5)$  to  $SU(3)$  have been determined for the  $^{152}\text{Sm}$ ,  $^{154}\text{Gd}$ , and  $^{156}\text{Dy}$  nuclei.

#### ACKNOWLEDGMENTS

We thank University of Kerbala, College of Science, Department of Physics and University of Mosul, College of Education for Pure Science, Department of Physics for supporting this work.

#### REFERENCES

1. A. Bohr and B. R. Mottelson, *Nuclear Structure* (World Sci, Singapore, 1998), Vol. 2.
2. F. Iachello and A. Arima, *The Interacting Boson Model* (Cambridge Univ. Press, Cambridge, 1987).
3. J. M. Arias, J. Dukelsky, J. E. García-Ramos, and J. Vidal, Phys. Rev. C **75**, 014301 (2007).
4. F. Iachello and N. V. Zamfir, Phys. Rev. Lett. **92**, 212501 (2004).
5. P. Cejnar, S. Heinze, and J. Dobeš, Phys. Rev. C **71**, 011304(R) (2005).
6. D. J. Rowe, Phys. Rev. Lett. **93**, 122502 (2004).
7. K. Abrahams, K. Allaart, and A. E. L. Dieperink, *Nuclear Structure* (Plenum Press, New York London, 1981).
8. A. Sethi, N. M. Hintz, D. N. Mihailidis, A. M. Mack, M. Gazzaly, K. W. Jones, G. Pauletta, L. Santi, and D. Goutte, Phys. Rev. C **44**, 700 (1991).
9. F. Iachello, Phys. Rev. Lett. **85**, 3580 (2000).
10. F. Iachello, Phys. Rev. Lett. **87**, 052502 (2001).
11. H. Ganev, V. P. Garistov, and A. I. Georgieva, Phys. Rev. C **69**, 014305 (2004).
12. H. G. Ganev, J. Phys.: Conf. Ser. **533**, 012015 (2014).
13. W. R. Phillips, I. Ahmad, H. Emling, R. Holzmann, R. V. F. Janssens, T.-L. Khoo, and M. W. Drigert, Phys. Rev. Lett. **57**, 3257 (1986).
14. R. K. Sheline and P. C. Sood, Phys. Rev. C **34**, 2362(R) (1986).
15. P. Schüler, Ch. Lauterbach, Y. K. Agarwal, J. De Boer, K. P. Blume, P. A. Butler, K. Euler, Ch. Fleischmann, C. Günther, E. Hauber, H. J. Maier, M. Marten-Tölle, Ch. Schandera, R. S. Simon, R. Tölle, and P. Zeyen, Phys. Lett. B **174**, 241 (1986).
16. D. Bonatsos, C. Daskaloyannis, S. B. Drenska, N. Karoussos, N. Minkov, P. P. Raychev, and R. P. Roussev, Phys. Rev. C **62**, 024301 (2000).
17. D. Bonatsos, P. E. Georgoudis, N. Minkov, D. Petrelis, and C. Quesne, Phys. Rev. C **88**, 034316 (2013).
18. H. Reşit Yazar, İ. Uluer, V. Ünaloglu, and S. Yaşar, Chin. J. Phys. **48**, 344 (2010).
19. C. Rangacharyulu, A. Richter, H. J. Wörtche, W. Ziegler, and R. F. Casten, Phys. Rev. C **43**, R949(R) (1991).
20. F. I. Sharrad, H. Y. Abdullah, N. AL-Dahan, A. A. Mohammed-Ali, A. A. Okhunov, and H. Abu Kassim, Rom. J. Phys. **57**, 1346 (2012).
21. H. R. Yazar, J Korean Phys Soc **47**, 592 (2005).
22. H. H. Khudher, A. K. Hasan, and F. I. Sharrad, AIP Conf. Proc. **1888**, 020030 (2017).
23. M. Baylan, Turk J Phys **25**, 369 (2001).
24. E. A. McCutchan, N. V. Zamfir, and R. F. Casten, Phys. Rev. C **69**, 064306 (2004).
25. M. L. Cescato, Y. Sun, and P. Ring, Nucl. Phys. A **533**, 455 (1991).
26. K. A. Hussain, M. K. Mohsin, and F. I. Sharrad, Ukr. J. Phys. **62** 653 (2017).
27. H. H. Kassim, Int. J. Mod. Phys. E **26**, 1750019 (2017).
28. M. A. Al-Jubbori, H. H. Kassim, F. I. Sharrad, A. At-tarzadeh, and I. Hossain, Nucl. Phys. A **970**, 438 (2018).
29. M. A. Al-Jubbori, H. H. Kassim, F. I. Sharrad, and I. Hossain, Int. J. Mod. Phys. E **27**, 1850035 (2018).
30. N. V. Zamfir and D. Kusnezov, Phys. Rev. C **63**, 054306 (2001).
31. I. M. Ahmed, M. A. Al-Jubbori, H. H. Kassim, H. Y. Abdullah, and F. I. Sharrad, Nucl. Phys. A **977**, 34 (2018).

32. I. M. Ahmed, G. N. Flaiyh, H. H. Kassim, H. Y. Abdullah, I. Hossain, and F. I. Sharrad, *Eur. Phys. J. Plus* **132**, 84 (2017).
33. R. F. Casten and D. D. Warner, *Rev. Mod. Phys.* **60**, 389 (1988).
34. H. H. Khudher, A. K. Hasan, and F. I. Sharrad, *Chin. J. Phys.* **55**, 1754 (2017).
35. A. Arima and F. Iachello, *Ann. Phys. (N.Y.)* **111**, 201 (1978).
36. F. I. Sharrad, H. Y. Abdullah, N. AL-Dahan, N. M. Umran, A. A. Okhunov and H. Abu-Kassim, *Chin. Phys. C* **37**, 034101 (2013).
37. M. A. Al-Jubbori, K. A. Al-Mtiuty, K. I. Saeed, and F. I. Sharrad, *Chin Phys C* **41**, 084103 (2017).
38. R. A. Sorensen, *Rev. Mod. Phys.* **45** 353 (1973).
39. A. A. Okhunov, F. I. Sharrad, A. A. Al-Sammarraie, and M. U. Khandaker, *Chin Phys C* **39**, 084101 (2015).
40. A. Shelley, I. Hossain, F. I. Sharrad, H. Y. Abdullah and M. A. Saeed, *Probl. At. Sci. Techn.* **64**, no. 3, 38 (2015).
41. S. M. Wong, *Introductory Nuclear Physics* (Prentice Hall Int, 1990).
42. D. Bonatsos, L. D. Skouras, and J. Rikowska, *Phys. Rev. C* **43**, 952R(R) (1991).
43. I. Hossain, I. M. Ahmed, F. I. Sharrad, H. Y. Abdullah, A. D. Salman, and N. AL-Dahan, *Chiang Mai J. Sci.* **42**, 996 (2015).
44. M. O. Waheed and F. I. Sharrad, *Nucl Phys At. Energy* **18**, 313 (2017).
45. M. A. Al-Jubbori, H. H. Kassim, F. I. Sharrad, and I. Hossain, *Nucl. Phys. A* **955**, 101 (2016).
46. I. Mamdouh and M. Al-Jubbori, *Indian J. Phys.* **89**, 1085 (2015).
47. P. H. Regan, C. W. Beausang, N. V. Zamfir, R. F. Casten, Jing-ye Zhang, A. D. Yamamoto, M. A. Caprio, G. Gurdal, A. A. Hecht, C. Hutter, R. Krücken, S. D. Langdown, D. A. Meyer, and J. J. Ressler *Phys. Rev. Lett* **90** 152502 (2003).
48. J. Engel and F. Iachello, *Phys. Rev. Lett.* **54**, 1126 (1985).
49. J. Engel and F. Iachello, *Nucl. Phys. A* **472**, 61 (1987).
50. A. Bohr and B. R. Mottelson, *Dan. Mat. Fys. Medd.* **27**(16) (1953).
51. G. Scharff-Goldhaber and J. Weneser, *Phys. Rev* **98** 212 (1955).
52. D. Bonatsos, *Phys. Lett. B* **200**, 1 (1988).
53. M. A. Al-Jubbori, F. Sh. Radhi, A. A. Ibrahim, S. A. Abdullah Albakri, H. H. Kassim, F. I. Sharrad, *Nucl. Phys. A* **971**, 35 (2018).
54. D. Bonatsos, A. Martinou, N. Minkov, S. Karampasia, and D. Petrellis, *Phys. Rev. C* **91**, 054315 (2015).
55. F. I. Sharrad, I. Hossain, I. M. Ahmed, H. Y. Abdullah, S. T. Ahmad, and A. S. Ahmed, *Braz. J. Phys.* **45**, 340 (2015).
56. H. H. Kassim and F. I. Sharrad, *Nucl. Phys. A* **933**, 1 (2015).
57. K. A. Hussain, M. K. Mohsin, and F. I. Sharrad, *Iran J. Sci. Technol. Trans. Sci.*, <https://doi.org/10.1007/s40995-017-0419-2>
58. W. N. Hussain and F. I. Sharrad, *J. Phys.: Conf. Ser.* **1032**, 012046 (2018).
59. H. H. Khudher, A. K. Hasan and F. I. Sharrad, *Ukr. J. Phys.* **62**, 152 (2017).
60. I. Hossain, H. H. Kassim, F. I. Sharrad, and A. S. Ahmed, *Sci. Asia* **42**, 22 (2016).
61. R. F. Casten and N. V. Zamfir, *Phys. Rev. Lett.* **87**, 052503 (2001).
62. R. F. Casten, *Roma. Rep. Phys.* **57**, 515 (2005).
63. I. Hossain, F. I. Sharrad, M. A. Saeed, H. Y. Abdullah, and S. A. Mansour, *Maejo Int. J. Sci. Technol.* **10**, 95 (2016).
64. <http://www.nndc.bnl.gov/chart/getENSDFData-sets.jsp>.
65. M. J. Martn, *Nucl. Data Sheets* **114**, 1497 (2013).
66. C. W. Reich, *Nucl. Data Sheets* **110**, 2257 (2009).
67. C. W. Reich, *Nucl. Data Sheets* **113**, 2537 (2012).
68. O. Scholten, *Computer code PHINT* (KVI, Groningen, 1980).
69. D. Kusnezov, *J. Phys. A* **22**, 4271 (1989).
70. D. Kusnezov, *J. Phys. A* **23**, 5673 (1990).
71. N. V. Zamfir and D. Kusnezov, *Phys. Rev. C* **67**, 014305 (2003).
72. H. H. Kassim, A. A. Mohammed-Ali, F. I. Sharrad, I. Hossain, and K. S. Jassim, *Iran J. Sci. Technol. Trans. Sci.* **42**, 993 (2018).
73. H. H. Kassim, A. A. Mohammed-Ali, M. A. Al-Jubbori, F. I. Sharrad, A. S. Ahmed, and I. Hossain, *J. Nat. Sci. Found. Sri Lanka* **46**, 3 (2018).
74. H. H. Kassim and F. I. Sharrad, *Int. J. Mod. Phys. E* **23**, 1450070 (2014).
75. M. O. Waheed and F. I. Sharrad, *Ukr. J. Phys.* **62**, 757 (2017).
76. M. A. Al-Jubbori, *Ukr. J. Phys.* **62**, 936 (2017).